Magnetoelastic coupling and unconventional magnetic ordering in the multiferroic triangular lattice $AgCrS_2$

F. Damay,[1,*] C. Martin,[2] V. Hardy,[2] G. André,[1] S. Petit,[1] and A. Maignan[2]
[1]*Laboratoire Léon Brillouin, CEA-CNRS UMR 12, F-91191 Gif-sur-Yvette Cedex, France*
[2]*Laboratoire CRISMAT, CNRS UMR 6508, 6 boulevard Maréchal Juin, F-14050 Caen Cedex, France*
(Received 9 February 2011; published 18 May 2011)

The temperature evolution of the crystal and magnetic structures of the ferroelectric sulfide $AgCrS_2$ has been investigated by means of neutron scattering. $AgCrS_2$ undergoes at $T_N = 41.6$ K a first-order phase transition, from a paramagnetic rhombohedral $R3m$ structure to an antiferromagnetic monoclinic structure with a polar Cm space group. In addition to being ferroelectric below T_N, the low-temperature phase of $AgCrS_2$ exhibits an unconventional collinear magnetic structure that can be described as double ferromagnetic stripes coupled antiferromagnetically, with the magnetic moment of Cr^{3+} oriented along b within the anisotropic triangular plane. The magnetic couplings stabilizing this structure are discussed using inelastic neutron scattering results. Ferroelectricity below T_N in $AgCrS_2$ can possibly be explained in terms of atomic displacements at the magnetoelastically induced structural distortion. These results contrast with the behavior of the parent frustrated antiferromagnet and spin-driven ferroelectric $AgCrO_2$.

DOI: 10.1103/PhysRevB.83.184413 PACS number(s): 75.25.−j, 61.05.fm

I. INTRODUCTION

Multiferroic materials, in which two or all three ferroic order parameters [ferroelectricity, (antiferro)magnetism, and ferroelasticity] are observed, have been the subject of intensive research in recent years. Such systems are rather rare in nature but are potentially interesting for a wide array of technological applications.[1,2] Magnetic transition-metal oxides with broken space-inversion symmetry represent one of the new classes of magnetoelectrics that are the most widely studied nowadays: in these "spin-driven ferroelectrics," it is the non collinear spiral spin structure that is responsible for the inversion symmetry breaking.[3,4] Examples of such oxides can be found among different structural families: perovskites [$TbMnO_3$ (Ref. 3)], spinels [$CoCr_2O_4$ (Ref. 5)], or delafossites [substituted $CuFeO_2$ (Refs. 6 and 7), $ACrO_2$ (A = Cu (Refs. 8 and 9), Ag (Ref. 10)], to cite only a few. For instance, in $CuCrO_2$, a modulated helicoidal magnetic structure derived from the 120° arrangement expected on a two-dimensional (2D) perfect triangular lattice is observed below $T_N = 24$ K,[8,11] and polarization in this compound probably arises[12] from a spin-orbit-coupling-induced modulation of the hybridization between the 3d cations carrying the spin (Cr^{3+}) and the ligand oxygen ions. Shedding light on the specific role of the anions in these compounds is therefore a key issue. Structurally closely related to the $ACrO_2$ delafossites with its stacking of regular triangular layers, the $ACrS_2$ series is seemingly an ideal system to investigate this matter. In addition, a multiferroic ground state has been recently reported in $AgCrS_2$.[13] In this context, the knowledge of the magnetic structure is of crucial importance, so as to validate the right physical model behind the multiferroic behavior. Surprisingly enough, although the magnetic structures of several $ACrS_2$ ($A = Cu^+$ (Refs. 14 and 15), Na^+ (Ref. 16), and Tl^+ (Ref. 17)] compounds with $R3m$ symmetry have been investigated in the past, $AgCrS_2$ still remains to be studied. This motivated our neutron powder diffraction study of $AgCrS_2$ in the temperature range 1.5–300 K, which is reported hereafter. We show that, at the antiferromagnetic ordering transition, this compound undergoes a first-order phase transition to a monoclinic ferroelectric phase; despite the stacked-triangular-layer topology of the compound, spins order collinearly within the layer planes, to form a stacking of double ferromagnetic stripes arranged antiferromagnetically [the so-called four-sublattice (4SL) or ↑↑↓↓ structure]. Preliminary inelastic neutron scattering results are discussed in the light of the possible magnetic exchange paths in the distorted structure, to understand the magnetic couplings involved in the stabilization of this unconventional magnetic ordering.

II. EXPERIMENT

5 g of polycrystalline $AgCrS_2$ were prepared by high-temperature solid state reaction. Powders of Ag, Cr, and S precursors were weighted according to the stoichiometric ratio. The resulting powder was carefully ground and pressed in the shape of bars, and heated in an evacuated silica tube at 900°C for 12 h. The obtained sample was then checked by room temperature x-ray diffraction and found to be single phase.

The magnetic susceptibility defined as $\chi = M/H$ was calculated from magnetization data measured in a magnetic field of 0.1 T, on warming from 1.5 to 300 K, after zero-field cooling, using a Quantum Design superconducting quantum interference device magnetometer. Heat capacity measurements were carried out in a physical property measurement system using a semiadiabatic relaxation method.[18] Outside the transition region, we used the standard 2τ model[19] to fit at once the heating and cooling branches at each point. Around the transition, however, a single-pulse method (SPM) suited to first-order transitions has been used.[20] In the SPM, the temperature is swept across the complete width of the transition, and the heat capacity is derived from a point-by-point analysis of the time response along each of the two branches.

Neutron powder diffraction (NPD) versus temperature was performed on the G4.1 diffractometer ($\lambda = 2.425$ Å) from 1.5

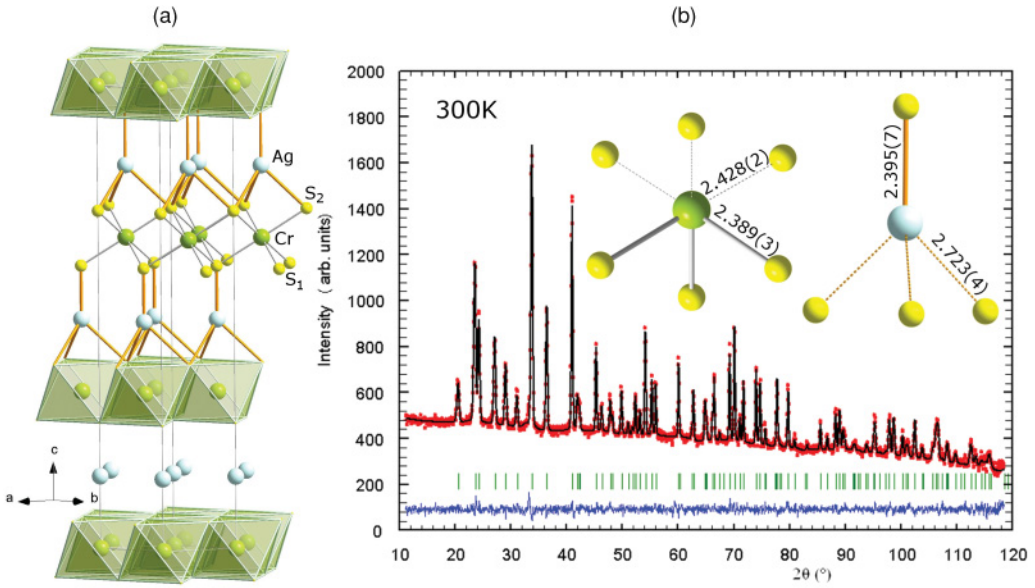

FIG. 1. (Color online) (a) $R3m$ crystal structure of $AgCrS_2$. (b) Refinement of the 3T2 neutron powder diffraction diffractogram of $AgCrS_2$ at 300 K (experimental data, open circles; calculated profile, continuous line; allowed Bragg reflections, vertical marks). The difference between the experimental and calculated profiles is displayed at the bottom of the graph. Inset: environments of Cr^{3+} and Ag^{+}.

to 300 K, and high-resolution neutron diffractograms were recorded on the diffractometer 3T2 ($\lambda = 1.225$ Å) at 10 and 300 K. Both diffractometers are located at LLB-Orphée (CEA-Saclay, France). Rietveld refinements and determination of the magnetic symmetry with representation analysis were performed with programs of the FULLPROF suite.[21] Inelastic neutron scattering experiments were performed on the thermal ($2T, k_f = 2.662\,Å^{-1}$) and cold ($4F2, k_f = 2.662$ or $1.550\,Å^{-1}$) neutron triple-axis spectrometers at LLB-Orphée (Saclay, France). Higher-order contaminations were removed with pyrolytic graphite or nitrogen-cooled Be filters placed in the scattered beam. Synchrotron diffractograms were recorded on the beamline I11 at the Diamond Light Source.

III. RESULTS

A. Room temperature crystal structure

In agreement with previous x-ray studies,[16,22,23] the refinement of the room temperature neutron data (3T2) confirms that $AgCrS_2$ has a rhombohedral noncentrosymmetric $R3m$ crystal structure (Fig. 1), with $a = b = 3.4979(1)$ Å and $c = 20.5369(9)$ Å. This structure can be described as a stacking of layers of edge-sharing octahedra $[CrS_2]_\infty$, connected through AgS_4 tetrahedra. Silver ions are ordered on half the tetrahedral sites, which form a pseudo-two-dimensional puckered honeycomb lattice. Unlike in the delafossite $R\bar{3}m$ structure of $AgCrO_2$,[24] the symmetry of the Cr^{3+} environment is not D_{3d} (which corresponds to a distorted octahedron where all Cr-O distances are equal) but C_{3v} : that is, a trigonal prism, with two sets of three equal Cr-S distances, 2.389(3) Å and 2.428(2) Å [inset of Fig. 1(b)]. The AgS_4 tetrahedron is also irregular, with one short [2.395(7) Å] and three long [2.723(4) Å] Ag-S distances [inset of Fig. 1(b)]. Within the regular triangular plane formed by the Cr^{3+} lattice, the Cr-Cr distance is 3.4979(1) Å, which is much larger than in chromium oxides with delafossite structure [2.9843(4) Å in $AgCrO_2$,[25] for example] but similar to that in $CuCrS_2$.[23] Results of the refinement, along with selected distances and angles, are summarized in Tables I and III. The anisotropic displacement factors U_{11} (displacement ellipsoid flattened along c) and U_{33} (displacement ellipsoid elongated along c) reported in Table I indicate that

TABLE I. Rietveld refinement results of the high-resolution neutron powder diffractogram of $AgCrS_2$ at 300 K [space group $R3m$ (no. 160, H setting) with all atoms on Wyckoff position 3a (0,0,z)].

Temperature	300 K
Space group	$R3m$ (no. 160)
Cell parameters (Å)	
a	3.4979(1)
b	3.4979(1)
c	20.5369(9)
Cell volume V (Å^3)	217.6(4)
Ag (0,0,z)	0.1545(2)
Cr (0,0,z)	0
S_1 (0,0,z)	0.2712(3)
S_2 (0,0,z)	0.7323(2)
$U_{\text{anisotropic}}$ (10^{-4} Å^2)	
Ag U_{11}	534(9)
Ag U_{33}	133(11)
Cr U_{11}	51(4)
Cr U_{33}	107(12)
$S_{1,2}$ U_{11}	64(3)
$S_{1,2}$ U_{33}	76(10)
Number of reflections	107
Number of parameters	16
Bragg R factor	3.21
χ^2	1.26

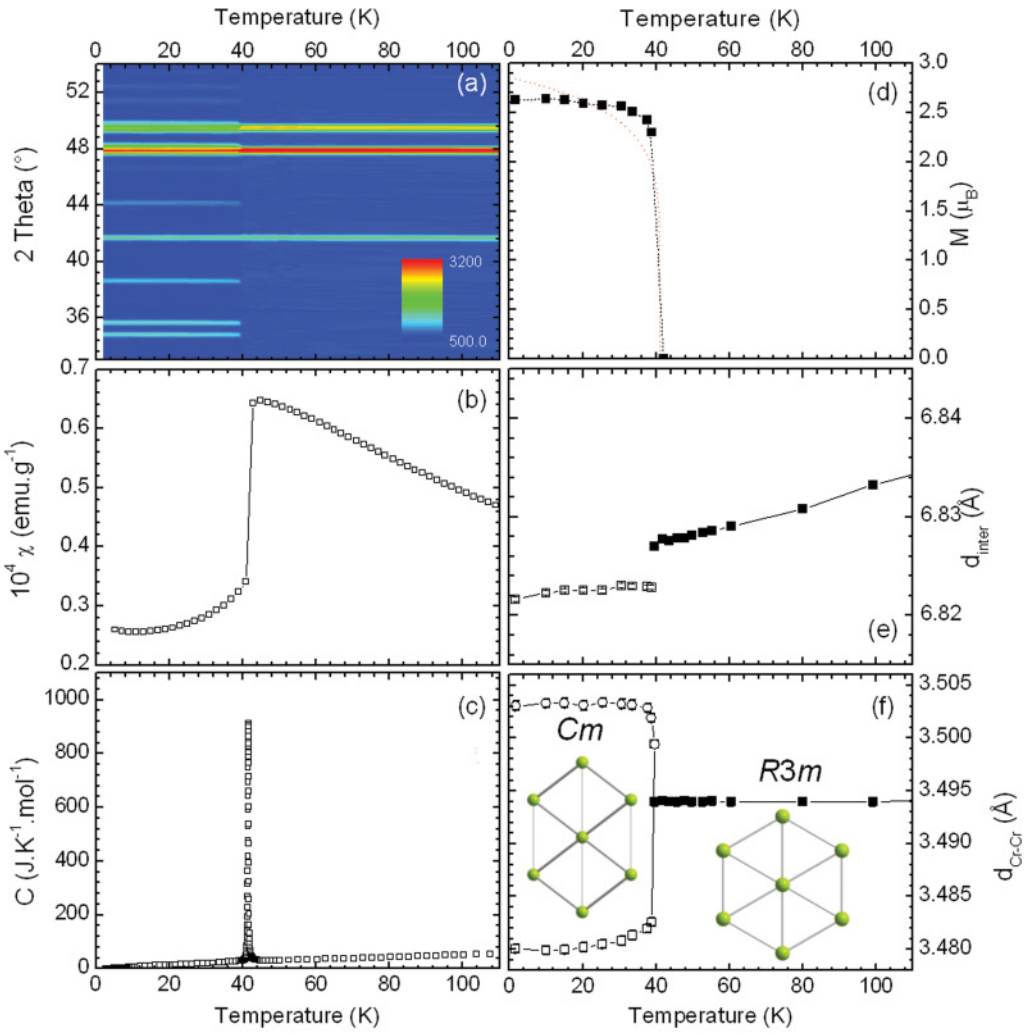

FIG. 2. (Color online): Temperature evolution of the G4.1 neutron diffractograms (a), of the zero-field-cooled susceptibility in 0.1 T (from Ref. 13) (b), of the specific heat (c), of the refined magnetic moment (d), of the distance between triangular planes d_{inter} (e), and of the Cr-Cr distances within the $[CrS_2]_\infty$ layer (f) of $AgCrS_2$. Lines are guides to the eye.

the atomic motion of Ag^+ is strongly anisotropic and confined within the (a, b) plane, a frequent feature among layered compounds.[26] The U_{11} displacement parameter of Ag^+ is actually exceptionally large; this has been reported previously for $AgCrS_2$, in studies related to its superionic conductivity at high temperature[27,29] in particular, for $AgCrSe_2$,[16,29] and to a lesser extent for $CuCrS_2$.[30] In Ref. 29, silver ions were shown to be strongly involved in low-frequency phonon modes corresponding to a vibration parallel to the $[CrS_2]_\infty$ layers. $AgCrS_2$ actually undergoes a reversible order-disorder ($R3m$-to-$R\bar{3}m$) phase transition around $T_C = 670$ K,[16] which corresponds to a statistical distribution of the Ag ions over all the tetrahedral positions between the $[CrS_2]_\infty$ layers in the high-temperature phase. Interestingly, $R3m$ is a polar space group (along $[111]_R$, that is, along c in the hexagonal cell), and ferroelectricity can be expected in $AgCrS_2$ below T_C. At room temperature, ferroelectricity is the result of the Cr plane being only slightly off centered between the two sulfur planes, and should actually be very sensitive to the position of Ag ions along c. The atomic disordering of the Ag^+ cations is likely therefore, as mentioned in Ref. 29, to preclude the observation of an electric polarization at room temperature.

B. Low-temperature crystal structure

The temperature dependence of the neutron diffractograms and of the susceptibility [Figs. 2(a) and 2(b)] in the 300–1.5 K range shows the appearance of antiferromagnetic Bragg peaks, concomitantly with a sharp decrease of χ, at $T_N = 41 \pm 1$ K, confirming the antiferromagnetic transition reported earlier.[13,31] The Curie-Weiss temperature extracted from a Curie-Weiss law fit between 150 and 400 K is in good agreement with previous results,[16,23] which report $\theta_{CW} = -55$ K, thus indicating predominantly antiferromagnetic interactions. The frustration parameter value $f = |\theta_{CW}|/T_N$ is about 1.3, which, as in $CuCrS_2$, is rather low for a triangular magnetic lattice.[31] The temperature evolution of the specific heat [Fig. 2(c)] exhibits a very sharp peak (full width at half maximum of ~0.25 K) at T_N, indicative of the first-order transition mentioned previously in Ref. 31. This is further supported by the observation of a temperature

TABLE II. Rietveld refinement results of the high-resolution neutron powder diffractogram of $AgCrS_2$ at 10 K [space group *Cm* (no. 8) with all atoms on Wyckoff position 2*a* (*x*, 0, *z*)].

Temperature	10 K
Space group	*Cm* (no. 8)
Cell parameters (Å)	
a	13.7861(2)
b	3.5042(1)
c	7.1132(1)
β (deg)	155.276(5)
Cell volume *V* (Å^3)	143.7(4)
Ag *x*	0.8459(8)
Ag *z*	0.1524(16)
Cr *x*	0
Cr *z*	0
S_1 *x*	0.7263(10)
S_1 *z*	0.2660(20)
S_2 *x*	0.2688(12)
S_2 *z*	0.7364(24)
$U_{isotropic}$ (10^{-4} Å^2)	
Ag	101(5)
Cr	75(6)
$S_{1,2}$	73(7)
Number of reflections	2311
Number of parameters	20
Bragg *R* factor	3.66
χ^2	2.27

TABLE III. Table III. Selected interatomic distances and angles in $AgCrS_2$ at 300 and 10 K (from high-resolution neutron powder diffractograms).

Temperature	300 K	10 K
Distances (Å)		
Ag-S_1	2.395(7)	2.41(7)
Ag-S_2	2.723(4) × 3	2.70(6)
		2.70(5) × 2
Cr-S_1	2.389(3) × 3	2.39(3)
		2.38(3) × 2
Cr-S_2	2.428(2) × 3	2.43(3)
		2.42(4) × 2
Cr-Cr_{in}	3.4979(4) × 6	3.5042(10) × 2
		3.4796(10) × 4
Cr-Cr_{out}	7.1373(1) × 6	7.1131(5) × 2
		7.1122(2) × 4
Cr-Cr_{in} (second neighbor)	6.0585(7) × 6	6.0125(2) × 2
		6.0553(1) × 4
CrS_2 layer thickness (Å)	2.624(6)	2.63(2)
AgS_4 height (Å)	4.222(6)	4.19(2)
Angles (deg)		
S-Cr-S_{in}	92.16(8)	92.51(4)
S-Cr-S_{out}	86.84(1)	87.24(4)
S-Ag-S	132.11(1)	131.8(5)

shift of about 0.2 K between the T_N recorded upon cooling ($T_N = 41.5$ K) and that recorded upon warming ($T_N = 41.7$ K, not shown). The Cr^{3+} ordered magnetic moment refined from the neutron data reaches $\sim 2.7\mu_B$, that is, 90% of its maximum value of $3\mu_B$, within 4 K [Fig. 2(d)].

The transition to the antiferromagnetic state occurs simultaneously with a structural transition involving a discontinuous contraction of the distance between triangular planes [Fig. 2(e)] and an anisotropic change of the Cr-Cr distances within the triangular plane [Fig. 2(f)], resulting in a lowering of the symmetry to monoclinic *Cm* [Fig. 3(a) and inset]. *Cm* is a subgroup of *R*3*m*, but, in agreement with the specific heat measurements, the order parameter expansion[32] contains a third-degree invariant so that, under the Landau condition,[33] this phase transition should indeed be first order. The monoclinic cell parameters at 10 K are $a = 13.7861(2)$ Å, $b = 3.5042(1)$ Å, $c = 7.1132(1)$ Å, and $\beta = 155.276(5)^\circ$, the relationship between the rhombohedral and the monoclinic cells being illustrated on Fig. 3(b). The result of the refinement of the high-resolution neutron powder diffractogram of the *Cm* phase at 10 K is illustrated on Fig. 3(a) and summarized in Tables II and III. Within the triangular plane, the distortion of the triangular lattice below T_N [Fig. 2(f)] leads to two long Cr-Cr distances along $[010]_m$ [3.5042(1) Å], and four short Cr-Cr distances of 3.4796(1) Å along $[\frac{1}{2}\frac{1}{2}1]_m$ and $[\frac{1}{2}\frac{\bar{1}}{2}1]_m$ [Fig. 3(c)]. If we now consider second-neighbor distances within the triangular plane, the monoclinic distortion leads to a shorter Cr-Cr distance along the $[102]_m$ direction [6.0125(2) Å], compared to 6.0553(1) Å along $[\frac{1}{2}\frac{3}{2}1]_m$ and $[\frac{1}{2}\frac{\bar{3}}{2}1]_m$. The Cr-Cr distances between triangular planes (Cr-Cr_{out} in Table III) decrease slightly in the monoclinic phase compared to the rhombohedral one; however, the difference between the two sets of Cr-Cr_{out} distances in the monoclinic phase lies within the experimental resolution, and their anisotropy as a result is far less pronounced than for the Cr-Cr_{in} distances, whether first or second neighbor. It should also be pointed out here that the Cr-S distances are kept almost unchanged through the transition, the variations observed lying within the experimental error.

The $R3m \rightarrow Cm$ phase transition has been further studied in terms of atomic displacements or modes,[34] to establish the instabilities at the origin of the distorted phase. Two macroscopic deformations are associated with the two irreducible representations of the space group *R*3*m* for $\mathbf{k}' = (000)$: a *c*-axis dilatation (or contraction), preserving the *R*3*m* symmetry (Γ_1), and a shear deformation in the *ac* plane (the polar plane of the *Cm* crystal class), which leads to the monoclinic *Cm* symmetry (primary mode Γ_3). Γ_1 leads to a compression of the AgS_4 tetrahedron and to a slight expansion of the $[CrS_2]_\infty$ layer thickness. The effect of Γ_3 is a shearing of the S_1 and S_2 planes, which breaks the C_{3v} symmetry of the CrS_6 octahedron. As a result of Γ_3, the polarization vector lies in the *ac* plane of the monoclinic cell, as there is an additional component of $\mathbf{P_S}$ parallel to the triangular plane. The amplitudes of these two modes are equivalent (0.0185 Å for the primary mode and 0.0252 Å for the secondary one) and rather large, almost comparable to those reported for archetypal ferroelectric materials,[35] and could explain the appearance of a spontaneous polarization in $AgCrS_2$ in its monoclinic phase.

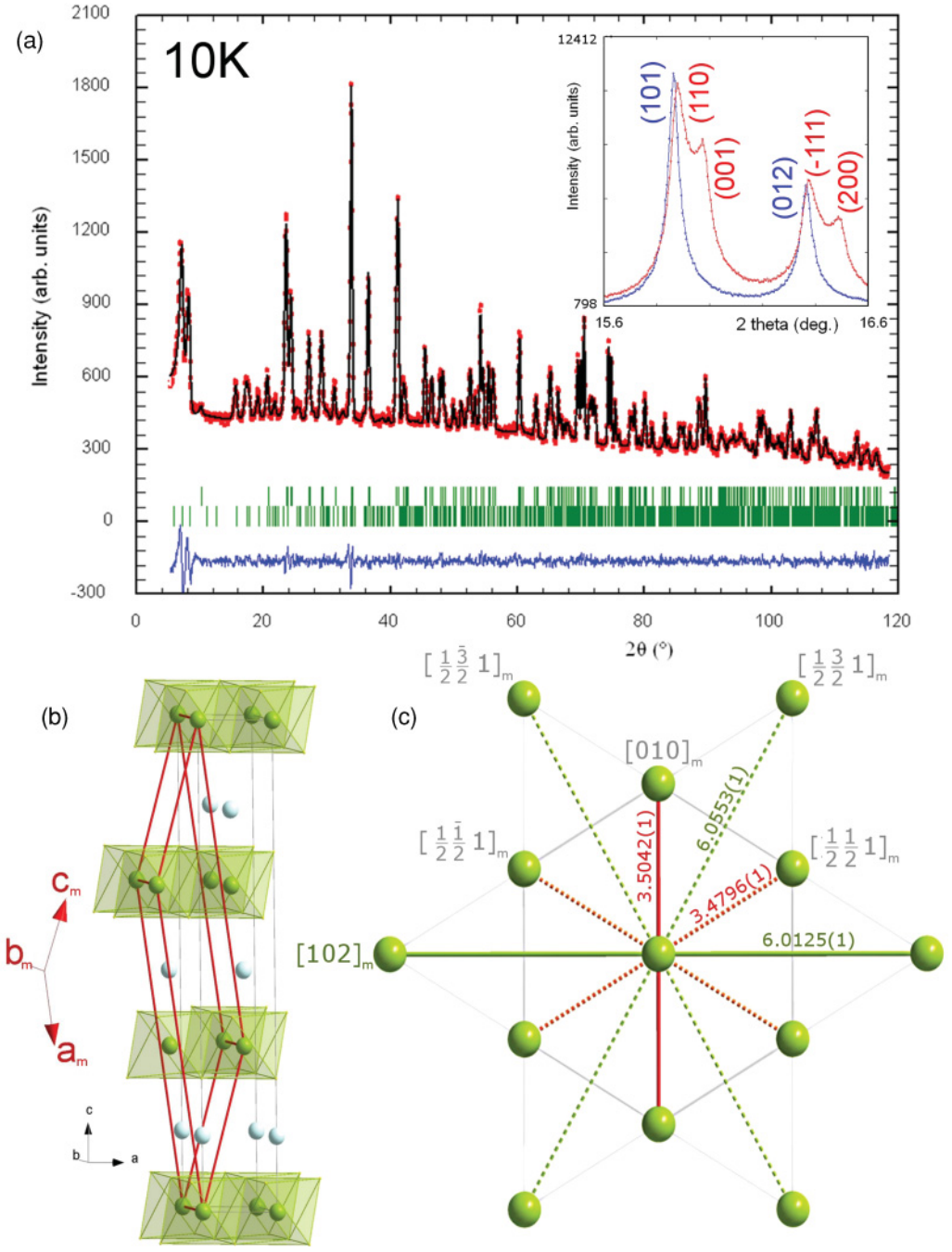

FIG. 3. (Color online) (a) Refinement of the 3T2 neutron powder diffraction diffractogram of $AgCrS_2$ at 10 K (experimental data, open circles; calculated profile, continuous line; allowed Bragg reflections, vertical marks). The difference between the experimental and calculated profiles is displayed at the bottom of the graph. Inset: Synchrotron x-ray data at 300 K (blue) and 15 K (red) evidencing the monoclinic structural distortion. (b) Relationship between the rhombohedral (thin grey lines) and the monoclinic cells (thick red lines). (c) Distances (in Å) at 10 K in the triangular plane. The cell distortion has been emphasized.

C. Magnetic structure

The magnetic Bragg peaks appearing below T_N can be indexed with a commensurate propagation vector $\mathbf{k} = (00\frac{1}{4})_m$. Symmetry analysis[21] shows that the magnetic representation is decomposed into two irreducible representations, $\Gamma_{\text{mag}} = \Gamma_1 \oplus 2\Gamma_2$. The corresponding basis vectors are $\psi_1 = (010)$ for Γ_1, and $\psi_{21} = (100)$ and $\psi_{22} = (001)$ for Γ_2. The only model compatible with the experimental data mixes two vectors transforming into Γ_1, $\psi_1 + i\psi_1$. The corresponding refinement ($T = 1.5$ K), which leads to a satisfying magnetic Bragg agreement factor of 6.5%, is illustrated on Fig. 4(a). The magnetic structure is collinear, and can be described within the triangular plane as ferromagnetically aligned double spin stripes running along b_m, which are arranged antiferromagnetically (4SL structure) [Fig. 4(b)]. The Cr^{3+} moment is oriented along b_m, and reaches $2.66(2)\mu_B$ at 1.5K.

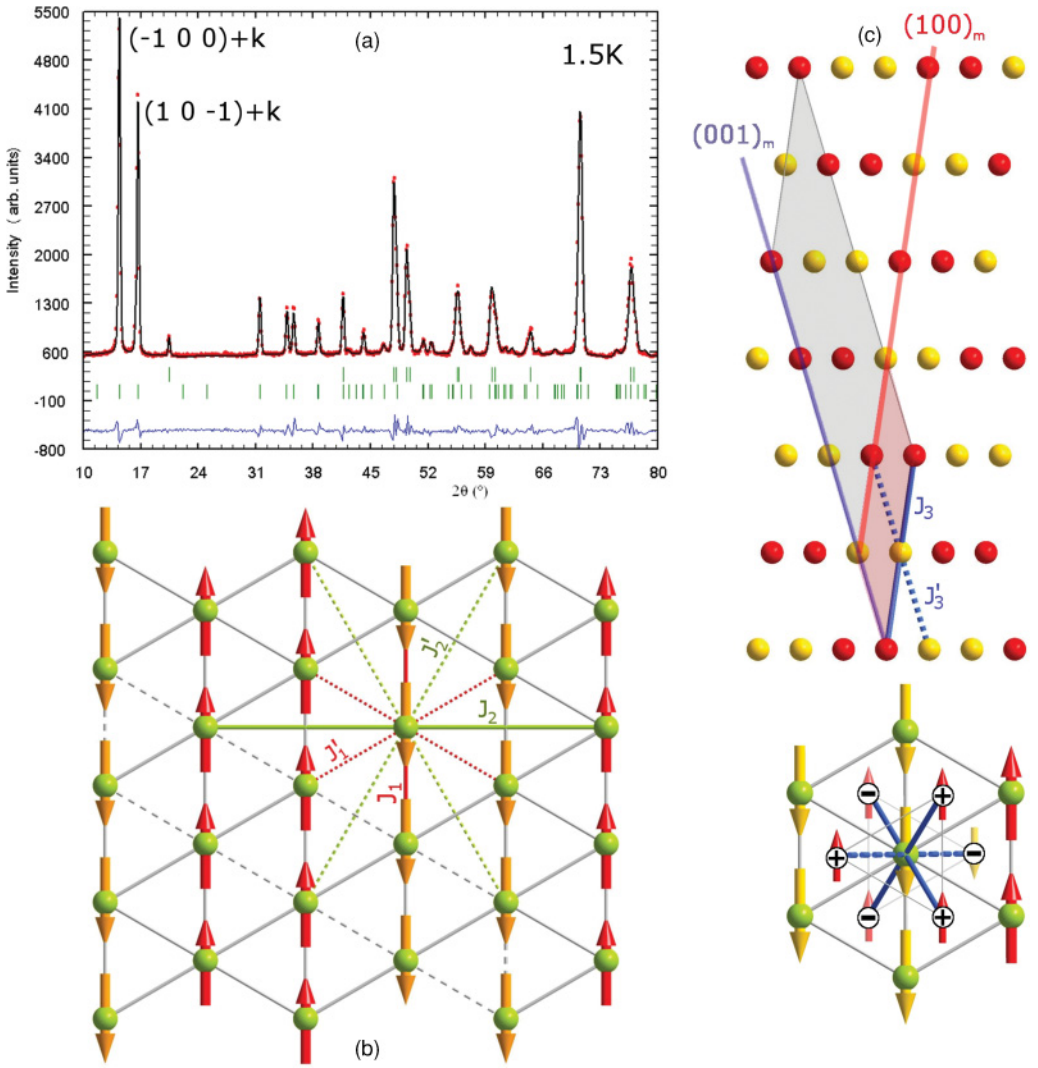

FIG. 4. (Color online) (a) Refinement of the G4.1 neutron diffraction data at 1.5 K (experimental data, open circles; calculated profile, continuous line; allowed Bragg reflections, vertical marks). The difference between the experimental and calculated profiles is displayed at the bottom of the graph. Magnetic peak indexing **H**+**k** is shown for the two main magnetic reflections. (b) Magnetic arrangement within the Cr^{3+} triangular lattice. (c) Projection of the magnetic structure along b_m (top) and along $[101]_m$ (bottom) illustrating the magnetic plane stacking (+ and − signs refer to spins belonging to the triangular plane directly above or underneath the reference one, respectively). The magnetic cell is shaded in gray, the crystal unit cell in red. In (b) and (c) dotted lines show degenerate directions along which the ↑↑↓↓ configuration is found. Full lines correspond to ferromagnetic (red lines) or in-plane (green) and interplane (blue) antiferromagnetic spin configuration. The color scheme is the same as in Fig. 3(c).

The stacking of the magnetic planes is shifted so that Cr^{3+} moments belonging to the $(001)_m$ plane are antiparallel along a_m [Fig. 4(c)]. Diffraction data measured above T_N also show a broad diffuse scattering signal around $Q_o = 0.6$ Å^{-1} (inset of Fig. 5), whose intensity gradually increases as the temperature nears T_N. As revealed by preliminary inelastic neutron scattering measurements, this diffuse scattering signal partly results from quasistatic fluctuations extending up to a few meV (Fig. 5), as at energy transfers $E = 3$ and 0.4 meV, the inelastic spectra also exhibit a broad maximum around Q_o. Interestingly, this Q_o value does not correspond to any of the magnetic Bragg peaks appearing below T_N (Fig. 5). To shed light on this issue, and assuming that the diffuse scattering $I(Q)$ arises from correlations between nearest-neighbor spins following Ref. 36, we can write $I(Q)$ as

$$I(Q) = F(Q)^2 \sum_{i,j} S_i S_j \frac{\sin Qr_{ij}}{Qr_{ij}},$$

where $F(Q)$ is the Cr form factor, S_i is the spin at site i, and r_{ij} is the distance between spins located on sites i and j. The maximum at Q_o yields a corresponding $r_{ij} = 6$–7 Å, clearly pointing out that the magnetic correlations do not arise from nearest-neighbor interactions on the triangular lattice: in such a case, with $r_{ij} = 3.5$ Å, we would expect $I(Q)$ to be maximum around 1.25 Å^{-1}. Following this simple model, spin correlations seem rather unexpectedly to arise from

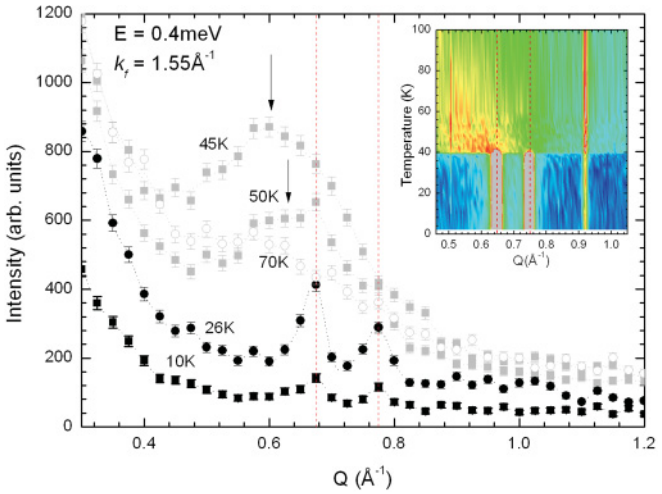

FIG. 5. (Color online) Temperature dependence of the inelastic scattering profiles at $E = 0.4$ meV ($k_f = 1.55$ Å^{-1}) of $AgCrS_2$. Inset: Temperature evolution of the diffraction profiles (G4.1 data) emphasizing the diffuse magnetic scattering around 0.6 Å^{-1} just above T_N. On both graphs the dotted red lines indicate the positions of the two magnetic Bragg peaks observed in this Q range below T_N.

second-neighbor (∼6.1 Å, Table III) and/or third-neighbor (∼6.9 Å) interactions.

On cooling below T_N, the diffuse scattering signal vanishes as the magnetic Bragg peaks appear (inset of Fig. 5). In parallel, the dynamic correlations at Q_o abruptly disappear and a new inelastic response, probably spin waves, emerges from the magnetic Bragg peaks (Fig. 5). The existence of a spin gap cannot be inferred from the inelastic data: a weak signal is still detected at very low energies, showing that if there is a gap, its value is smaller than 0.4 meV. It seems therefore that Cr^{3+} retains its Heisenberg character, as in $CuCrO_2$.[9] The dispersion (not shown) is very steep, but further measurements, currently in progress, are required to obtain a more accurate picture of the spin dynamics.

IV. DISCUSSION

The first-order structural transition that occurs simultaneously with collinear antiferromagnetic ordering in $AgCrS_2$ is a strong indication of spin-lattice coupling, a behavior that was reported recently in $CuCrS_2$ as well.[15] The observation of a macroscopic polarization value at $T < T_N$ in this material stresses in addition that the electric dipole is coupled to the magnetic moment through the lattice. In this framework, the polarization measured by Singh *et al.*[13] in $AgCrS_2$ seems to be reasonably interpreted on the basis of charge displacement at T_N, and more precisely of the shearing of the sulfur planes. To use the classification of multiferroics proposed by Cheong and Mostovoy,[37] and in contrast to closely structurally related compounds like $AgCrO_2$ or $CuCrO_2$,[10] $AgCrS_2$ does not appear to belong to the class of spin-driven ferroelectrics, in which ferroelectricity results from noncollinear magnetic ordering. $AgCrS_2$ belongs rather to the geometric ferroelectric class,[37] in which polarization becomes measurable following a lattice distortion induced by the magnetic ordering.

The magnetic structures of several $ACrS_2$ (A = Li^+,Cu^+,Na^+,K^+,Tl^+) compounds have been investigated in the past, and show a wide variety of magnetic arrangements: for the largest A radius, ferromagnetism has been reported [$A = Tl^+$ (Ref. 17)], as well as ferromagnetic layers coupled antiferromagnetically [$A = K^+$ (Ref. 38)]. A 120° helicoidal magnetic structure is known for the smallest A [$A = Li^+$ (Ref. 39)]. Incommensurate helicoidal magnetic structures have also been reported for $A = Na^+$ (Ref. 16) and Cu^+;[14,15] $AgCrS_2$ seems therefore to be the first example in this family of the four-sublattice antiferromagnetic structure.

The occurrence of an up-up-down-down structure on a triangular plane still remains puzzling. In a topologically rather similar compound, $CuFeO_2$, a ↑↑↓↓ configuration has been reported below $T_N = 11$ K, simultaneously with a first-order lattice distortion from $R\bar{3}m$ to $C2/m$.[40] The magnetic exchanges that could stabilize such a structure are still hypothetical, and the authors invoke a third-neighbor interaction inside the triangular plane, in reference to the phase diagram of the 2D Ising spin on a triangular lattice.[41] The magnetic arrangement in the triangular plane is different [$\mathbf{k} = (0\frac{1}{2}\frac{1}{2})$], however, from the one observed in $AgCrS_2$, as the magnetic coupling along b_m is antiferromagnetic.

The strong magnetoelastic coupling that is observed in $AgCrS_2$ could provide a way to understand the dominant magnetic exchanges stabilizing this complex magnetic structure: indeed, we observe that the monoclinic distortion induces two nonequivalent nearest-neighbor couplings J_1 and J_1', as well as two nonequivalent second-neighbor couplings (J_2 and J_2') [see the full and dotted lines on Figs. 3, 4(b) and 4(c)]. The observed four-sublattice spin arrangement cancels the effect of J_1' and J_2', withdrawing the molecular field due to both couplings. We can therefore speculate that the relevant magnetic interactions are those that correspond to the remaining unfrustrated pathways, the ferromagnetic first-neighbor coupling J_1 (along b_m), the antiferromagnetic second-neighbor super-superexchange J_2 (along Cr-S_1-S_2-Cr, perpendicular to b_m), and the interplane antiferromagnetic super-superexchange J_3 (along a_m). Although the impact of the monoclinic distortion actually only subtly affects distances and angles, it is enough to lift the degeneracy between magnetic exchange paths and thus favors one magnetic configuration. Incidentally, a similar analysis holds in the case of the ↑↑↓↓ arrangement observed in $CuFeO_2$. Our inelastic scattering results also emphasize in addition the relevance of J_2 and/or J_3 couplings *above* T_N, as they correspond to interactions between Cr spins between 6 and 7 Å apart, which will give scattering around $Q = 0.6$ Å^{-1}.

The fact that for large Cr-Cr distances ferromagnetic coupling is observed can be understood within the framework of Goodenough's model, which is based on a competition between direct cation-cation exchange and super cation-anion-cation exchange.[42] The direct Cr-Cr exchange across the common edges of adjacent CrS_6 octahedra involves half-filled t_{2g} orbitals of the Cr^{3+} ions, and thus favors antiferromagnetic coupling. Superexchange through Cr-S-Cr with a close to 90° angle involves a half-filled t_{2g} orbital of a cation, an empty e_g orbital of the second cation, and an anionic p orbital, thus favoring ferromagnetic coupling. Direct exchange is more sensitive to the distance between cations than superexchange, and

for a threshold value of the Cr-Cr distance, indirect exchange will start to predominate, thus leading to a ferromagnetic arrangement of the Cr moments. Rosenberg *et al.*[17] evaluated this threshold value to be ∼3.6 Å: in $AgCrS_2$, ferromagnetic spin arrangement is observed for Cr-Cr = 3.5042(10) Å. The role of the ligand anion in the magnetic couplings in this material is still a matter of speculation, but it should provide a most interesting field of future research, on both experimental and theoretical grounds.

V. CONCLUSION

The investigation of $AgCrS_2$ by neutron scattering techniques has evidenced a magnetoelastic-coupling-induced structural transition at T_N, toward a polar monoclinic phase. The antiferromagnetic arrangement is rather unusual compared to $CuCrS_2$ or to frustrated parent delafossite compounds like $AgCrO_2$, and can be described as double ferromagnetic stripes coupled antiferromagnetically, running along $[010]_m$. How this magnetic structure is stabilized can be understood using a ferromagnetic coupling along b_m (the direction which corresponds to the largest Cr-Cr distance in the anisotropic triangular lattice) in addition to an antiferromagnetic second-neighbor coupling perpendicular to b_m, which could be the driving force behind the structural distortion.

ACKNOWLEDGMENTS

The authors acknowledge F. Porcher for neutron diffraction experiments on 3T2 (LLB-Orphée). Part of this work was also carried out with the support of the Diamond Light Source and we thank C. Tang and S. Thompson for their help during the experiment. Financial support for this work was partially provided by the French Agence Nationale de la Recherche, Grant No ANR-08-BLAN-0005-01.

*francoise.damay@cea.fr

[1] M. Fiebig, J. Phys. D **38**, R123 (2005).
[2] R. Ramesh and N. A. Spaldin, Nature Mater. **6**, 21 (2007).
[3] T. Kimura, T. Goto, H. Shintani, K. Ishizaka, T. Arima, and Y. Tokura, Nature (London) **426**, 55 (2003).
[4] N. Hur, S. Park, P. A. Sharma, J. S. Ahn, S. Guha, and S. W. Cheong, Nature (London) **429**, 392 (2004).
[5] Y. Yamasaki, S. Miyasaka, Y. Kaneko, J. P. He, T. Arima, and Y. Tokura, Phys. Rev. Lett. **96**, 207204 (2006).
[6] T. Kimura, J. C. Lashley, and A. P. Ramirez, Phys. Rev. B **73**, 220401 (2006).
[7] N. Terada, T. Nakajima, S. Mitsuda, H. Kitazawa, K. Kaneko, and N. Metoki, Phys. Rev. B **78**, 014101 (2008).
[8] M. Poienar, F. Damay, C. Martin, V. Hardy, A. Maignan, and G. André, Phys. Rev. B **79**, 014412 (2009).
[9] M. Poienar, F. Damay, C. Martin, J. Robert, and S. Petit, Phys. Rev. B **81**, 104411 (2010).
[10] S. Seki, Y. Onose, and Y. Tokura, Phys. Rev. Lett. **101**, 067204 (2008).
[11] Y. Oohara, S. Mitsuda, H. Yoshizawa, N. Yaguchi, H. Kuriyama, T. Asano, and M. Mekata, J. Phys. Soc. Jpn. **63**, 847 (1994).
[12] T. H. Arima, J. Phys. Soc. Jpn. **76**, 073702 (2007).
[13] K. Singh, A. Maignan, C. Martin, and C. Simon, Chem. Mater. **21**, 5007 (2009).
[14] M. Wintenberger and Y. Allain, Solid State Commun. **64**, 1343 (1987).
[15] J. C. E. Rasch, M. Boehm, C. Ritter, H. Mutka, J. Schefer, L. Keller, G. M. Abramova, A. Cervellino, and J. F. Loffler, Phys. Rev. B **80**, 104431 (2009).
[16] F. Engelsman, G. A. Wiegers, F. Jellinek, and B. Vanlaar, J. Solid State Chem. **6**, 574 (1973).
[17] M. Rosenberg, A. Knülle, H. Sabrowsky, and C. Platte, J. Phys. Chem. Solids **43**, 87 (1982).
[18] Quantum-Design, PPMS Heat Capacity Option User's Manual, San Diego, January 2009.
[19] J. S. Hwang, K. J. Lin, and C. Tien, Rev. Sci. Instrum. **68**, 94 (1997).
[20] V. Hardy, Y. Breard, and C. Martin, J. Phys.: Condens. Matter **21**, 075403 (2009).
[21] J. Rodriguez-Carvajal, Physica B **192**, 55 (1993).
[22] H. Hahn and C. De Lorent, Z. Anorg. Allg. Chem. **290**, 68 (1957).
[23] P. F. Bongers, C. VanBrugg, J. Koopstra, W. P. F. Omloo, G. A. Wiegers, and F. Jellinek, J. Phys. Chem. Solids **29**, 977 (1968).
[24] E. Gehle and H. Sabrowsky, Z. Naturforsch. B **30**, 659 (1975).
[25] R. D. Shannon, D. B. Rogers, and C. T. Prewitt, Inorg. Chem. **10**, 713 (1971).
[26] J. S. O. Evans, J. Chem. Soc. Dalton Trans. 3317 (1999).
[27] M. S. Whittingham, Prog. Solid State Chem. **12**, 41 (1978).
[28] A. G. Gerards, B. A. Boukamp, and G. A. Wiegers, Solid State Ionics **9–10**, 471 (1983).
[29] P. Brüesch, T. Hibma, and W. Bührer, Phys. Rev. B **27**, 5052 (1983).
[30] N. Le Nagard, G. Collin, and O. Gorochov, Mater. Res. Bull. **14**, 1411 (1979).
[31] H. Kawaji, T. Atake, and Y. Saito, J. Phys. Chem. Solids **50**, 215 (1989).
[32] H. Stokes and D. Hatch, www.physics.byu.edu/stokesh/isotropy.html.
[33] L. Landau and E. Lifshitz, *Statistical Physics* (Pergamon, New York, 1980), Chap. 14.
[34] D. Orobengoa, C. Capillas, M. I. Aroyo, and J. M. Perez-Mato, J. Appl. Crystallogr. **42**, 820 (2009).
[35] R. W. Wyckoff, *Crystal Structures* (Krieger Publishing, New York, 1963).
[36] E. F. Bertaut and P. Burlet, Solid State Commun. **5**, 279 (1967).
[37] S. W. Cheong and M. Mostovoy, Nature Mater. **6**, 13 (2007).
[38] B. Vanlaar and F. Engelsman, J. Solid State Chem. **6**, 384 (1973).
[39] B. Vanlaar and D. J. W. Ijdo, J. Solid State Chem. **3**, 590 (1971).
[40] F. Ye, Y. Ren, Q. Huang, J. A. Fernandez-Baca, P. C. Dai, J. W. Lynn, and T. Kimura, Phys. Rev. B **73**, 220404 (2006).
[41] T. Takagi and M. Mekata, J. Phys. Soc. Jpn. **64**, 4609 (1995).
[42] J. B. Goodenough, *Magnetism and the Chemical Bond* (Interscience, New York, 1963).